

# Listening for the Axion Echo with the 21 CentiMeter Array

Ariel Arza<sup>a,b</sup>, Quan Guo<sup>c</sup>, Lei Wu<sup>b</sup>, Qiaoli Yang<sup>d</sup>, Xiaolong Yang<sup>c,e</sup>, Qiang Yuan<sup>f,g</sup> and Bin Zhu<sup>h</sup>

<sup>a</sup>*Tsung-Dao Lee Institute and School of Physics and Astronomy,  
Shanghai Jiao Tong University, Shanghai 200240, China*

<sup>b</sup>*Department of Physics and Institute of Theoretical Physics,  
Nanjing Normal University, Nanjing 210023, China*

<sup>c</sup>*Shanghai Astronomical Observatory, Chinese Academic Science, Shanghai 200030, China*

<sup>d</sup>*Department of Physics and Siyuan Laboratory, Jinan University, Guangzhou 510632, China*

<sup>e</sup>*Shanghai Key Laboratory of Space Navigation and Positioning Techniques, Shanghai 200030, China*

<sup>f</sup>*Key Laboratory of Dark Matter and Space Astronomy,  
Purple Mountain Observatory, Chinese Academy of Sciences, Nanjing 210023, China*

<sup>g</sup>*School of Astronomy and Space Science, University of Science and Technology of China, Hefei 230026, China*

<sup>h</sup>*Department of Physics, Yantai University, Yantai 264005, China*

(Dated: September 14, 2023)

The axion is a hypothetical elementary particle that could solve the long-standing strong CP problem in particle physics and the dark matter mystery in the cosmos. Due to the stimulation of the ambient photons, the axion dark matter decay into photons is significantly enhanced so that its echo signal could be detected by terrestrial telescopes. As a pathfinder, we study the expected sensitivity of searching for the axion dark matter in the mass range between 0.41 and  $1.6\mu\text{eV}$  with the 21 CentiMeter Array (21CMA). We aim to cover the whole 21CMA frequency range in two years by using a 1MW emitter. We find that the resulting sensitivity on the axion-photon coupling could surpass other existing limits by about one order of magnitude.

## I. INTRODUCTION

Dark matter (DM) constitutes approximately 84.4% of the total matter and 26.4% of the Universe's energy density, and its identification remains one of the most significant puzzles in the nature [1]. The quantum chromodynamics (QCD) axion is a prominent DM candidate that offers an elegant solution to the strong CP problem [2–6] and naturally saturates the required DM energy density [7]. Additionally, axion-like particles (ALPs) are predicted by models featuring global  $U(1)$  symmetry breaking, such as those appearing in string theory compactifications [8, 9], and have the potential to explain many unresolved puzzles in particle physics and cosmology.

In the context of the early universe, the misalignment mechanism and the decay of topological defects enabled the non-thermal production of QCD axions and ALPs [10–13]. The mass range of these particles, which is crucial for realizing the cold dark matter abundance, depends on whether the PQ symmetry was broken before or after inflation [14, 15]. For the ALPs, the mass range can be from  $10^{-22}$  to  $\sim 1\text{eV}$  [16].

Several resonant cavity experiments, such as those conducted by the ADMX collaboration [17], are currently the most sensitive for detecting dark matter axions, having excluded QCD axion models in the mass range of  $2.66 - 4.2\mu\text{eV}$  [18–20]. Other experiments, such as HAYSTAC [21], CAPP [22, 23], and QUAX [24], are actively working to improve their sensitivity. For lower axion masses, several resonant and broadband experiments, including ABRACADABRA [25], SHAFT [26], BASE [27], and DANCE [28], are available. For even lower masses, axions can be detected through their mag-

netic activity at the Earth's surface [29–31]. Future projects, such as MADMAX [32], DM Radio [33], GrA-Hal [34], APLHA [35], BREAD [36], LAMPOST [37], SRF [38, 39], TOORAD [40, 41], and WISPLC [42], aim to detect axions and contribute to the ongoing efforts to uncover the nature of dark matter. For complete reviews on updated axion phenomenology, see Refs. [43, 44].

Axions, with mass  $m_a$ , are capable of spontaneously decaying into two photons, each with energy  $m_a/2$  in the axion rest frame. The estimated average lifetime of a single axion is more than 30 orders of magnitude greater than the age of the universe, at  $10^{41}\text{yr}$ , for a typical dark matter QCD axion [13]. Even for a more visible axion-like particle with a mass of  $m_a = 10^{-5}\text{eV}$  and a coupling constant of  $g = 10^{-11}\text{GeV}^{-1}$ , the lifetime is still substantial at  $10^{34}\text{yr}$ . However, the presence of an initial photon background with photon energy  $m_a/2$  can significantly reduce the lifetime of the axion, implying enhanced signals [45] and parametric resonant instabilities [46–49]. This is due to the property of Bose statistics, which allows for numerous bosons to occupy the same phase space state. To be more specific, a photon occupancy number  $f_\gamma$  increases the axion decay rate by a factor  $1 + f_\gamma$ . For instance, a photon background intensity of  $1\text{kW/m}^2$ , at frequency 1GHz and bandwidth 1MHz, gives  $f_\gamma \sim 10^{19}$ . As a result, the axion decay can be dramatically more likely, producing an axion dark matter echo that propagates backwards with respect to the photon background direction [50, 51].

In this paper, we propose to utilize the 21 CentiMeter Array (21CMA) observatory in China to probe axion echo signals in the frequency range  $50 - 200\text{MHz}$ , corresponding to axion masses in the range  $4.13 \times 10^{-7}\text{eV} <$

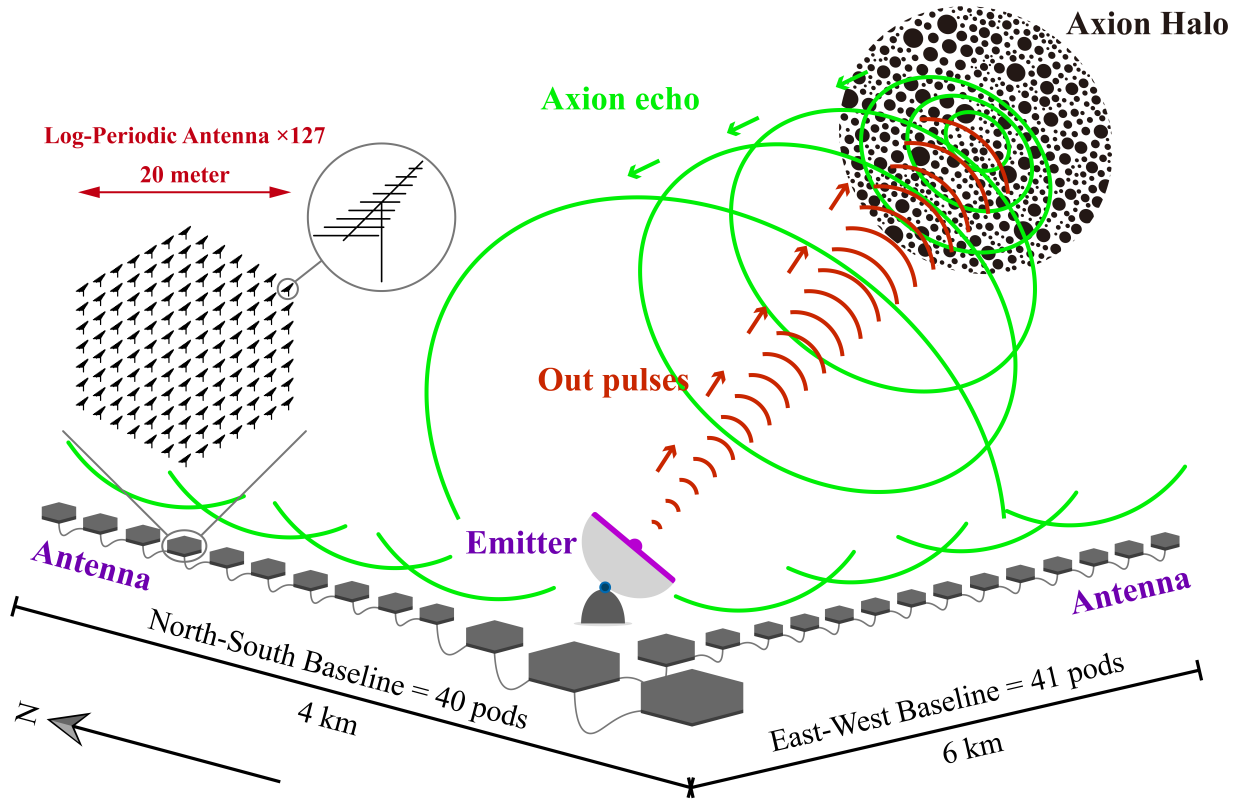


FIG. 1. Sketch map of using the 21 Centimeter Array in Xinjiang, China, and an emitter to activate axion and capture corresponding echo emissions. The map displays the location of the two primary components of the array: the North-South Baselines and the East-West Baselines. The 21CMA is a radio interferometer designed to study the large-scale structure of the universe and the epoch of reionization. This figure provides a visual representation of the site and its components, which are critical for the success of the 21CMA's scientific goals. In particular, the figure illustrates the potential to detect axion echoes at the 21CMA site by emitting a powerful beam into the sky.

$m_a < 1.65 \times 10^{-6} \text{ eV}^1$ . We aim to employ a 1MW emitter, assuming a total integration time of 2 years to cover the whole 21CMA frequency range. In contrast with the proposals for astrophysical observations [45, 52–54], and optical experimental setups [55], our proposal works as an option for lower axion masses and it is also more sensitive up to about one order of magnitude in the axion-photon coupling.

## II. EXPERIMENTAL SETUP AND SIGNAL POWER

The basic setup of the experiment includes a radio emitter and a receiving antenna array with specific layout (see details below). The emitter sends a beam of radio waves with power  $P_0$  and physical size (area)  $S_0 = \pi R_0^2$ .

The beam is collimated by a dish antenna of radius  $R_0$ , where we assume a full efficiency of the dish.

For an emitter turned on during a time  $t_{\text{on}}$ , the echo intensity, as a function of polar coordinates  $\vec{r} = (r, \theta)$  and time  $t$ , for a particular axion transverse velocity  $\vec{v}_\perp$  is

$$I(r, \theta, v_\perp, t) = \frac{\pi}{32\sqrt{2}} \frac{g^2 \rho P_0 R_0}{\Delta S_0 v_\perp} \exp\left(\frac{-r^2 \sin^2 \theta}{R_0^2}\right) \times \begin{cases} \text{erf}\left(\frac{r \cos \theta}{R_0}\right) + \text{erf}\left(\frac{v_\perp t - r \cos \theta}{R_0}\right) & \text{for } t < t_{\text{on}} \\ \text{erf}\left(\frac{v_\perp t - r \cos \theta}{R_0}\right) - \text{erf}\left(\frac{v_\perp (t - t_{\text{on}}) - r \cos \theta}{R_0}\right) & \text{for } t > t_{\text{on}} \end{cases}, \quad (1)$$

where  $\rho$  represents the local axion energy density and  $g$  is the effective axion-photon coupling. Here, the polar coordinates are defined such that  $\theta$  is the angle between  $\vec{r}$  and  $\vec{v}_\perp$ .

The echo is produced from the interaction of a photon beam with frequency bandwidth  $\delta\nu$  and the axion local energy density with momentum dispersion  $\delta\vec{p}$ . The parameter  $\Delta$  accounts for the maximum between these two dispersions, thus it can be written as  $\Delta = \sqrt{(2\pi\delta\nu)^2 + (\delta p_\parallel/2)^2}$ , where  $\parallel$  refers to the component

<sup>1</sup> The radio astronomy frequency window (where the sky is transparent to radio/micro waves) ranges, approximately, from 30 MHz to 30 GHz, which corresponds to axion masses within the range  $2.5 \times 10^{-7} - 2.5 \times 10^{-4} \text{ eV}$ .

parallel to the beam wave vector.

Averaging over the axion transverse velocity distribution  $f_a(v_\perp)$ , we have

$$\bar{I}(r, t) = \int_0^\infty v_\perp dv_\perp f_a(v_\perp) \int_0^{2\pi} d\theta I(r, \theta, v_\perp, t), \quad (2)$$

where we assume the standard halo model (SHM) Maxwell-Boltzmann velocity distribution

$$f_a(\vec{v}_\perp) = \frac{3}{2\pi\sigma_v^2} e^{-\frac{3v_\perp^2}{2\sigma_v^2}}, \quad (3)$$

with  $\sigma_v = 270$  km/s being the DM velocity dispersion. It is worth saying that the axion dark matter echo method can be very sensitive for some particular models of the dark matter phase space distribution, such as the caustic ring model [56, 57], the Earth halo model [58], and the presence of fine grained streams [59, 60]. However, for testing these models we need special experimental treatment which is out of the scope of this work.

The time profile of the echo power signal collected by a receiving array can be computed as

$$P(t) = \int_0^\infty dr r \int_0^{2\pi} d\phi \bar{I}(r, t) w(r, \phi). \quad (4)$$

Here  $w(r, \phi)$  represents the weight of the array layout, which is 1 for spatial locations with an antenna and 0 without the antenna. The spatial distribution of the echo signal averaged within any time interval  $T$  is

$$F(r) = \frac{1}{T} \int_0^T dt \bar{I}(r, t). \quad (5)$$

We take the 21CMA as an example of the receiving array. The 21CMA is a unique low-frequency radio interferometer, which locates in the Tianshan Mountains in western China<sup>2</sup>. This ground-based meter-wave interferometric array is designed to probe the 21 cm radiation of neutral hydrogen from the cosmic dawn and the epoch of reionization at  $z = 6 \sim 27$ . It was constructed from August 2005 to July 2006 and upgraded by July 2010. The array consists of 81 pods with 127 log-periodic antennas each, deployed along two perpendicular arms of  $6 \times 4$  km in length (see the first panel of Fig. 2). The array images a field of  $10 \sim 100$  square degrees centered on the North Celestial Pole 24 hours per day in the low frequency range of 50 MHz to 200 MHz with a resolution of 24 kHz [61, 62]. To optimize the detection of the axion echo, we also consider a re-arrangement of the 21CMA layout to a hexagon shape (with an addition of 10 pods to make a symmetric shape), as shown in the second panel of Fig. 2.

The third panel of Fig. 2 shows the spatial distribution of the echo signal  $F(x, y) = F(r, \phi)$ , averaged over  $t_{\text{on}}$ . The distribution features the expected circular shape and follows a  $1/r$  behavior. The fourth panel of Fig. 2 presents the time dependence of the power signal  $P(t)$ , for  $t_{\text{on}} = 1$  s and the layouts of the current 21CMA (dashed) and the optimized re-arrangement (solid). To get these profiles, we have assumed a signal frequency of  $\nu = 100$  MHz and an axion-photon coupling  $g = 10^{-10} \text{ GeV}^{-1}$ . The arms of the 21CMA have a length of a few kilometers, so the signal reaches a saturation value after a time of  $t_{\text{sat}} \sim$  tens of milliseconds. If  $t_{\text{on}} < t_{\text{sat}}$ , the signal would start to decline before reaching the saturated value. The results further show that the optimization of the array layout gives a factor of  $\sim 5.8$  enhancement of the echo power, due to a higher collection efficiency of the optimized layout for an isotropic signal distribution.

### III. PROJECTED SENSITIVITY

In the laboratory frame, the outgoing photon frequency required for stimulated axion decay is given by  $\nu = m_a/(4\pi)(1 + v_\parallel)$ , where  $v_\parallel$  is the axion velocity component parallel to the beam wave vector. The resulting echo signal is a spectral line at frequency  $\nu_e = m_a/(4\pi)(1 - v_\parallel)$ . When assuming the standard halo model (SHM), the echo line width is  $\delta\nu_e = \delta v_\parallel \times \nu = 5.21 \times 10^{-4} \nu$  for a wide outgoing beam bandwidth, and equal to the beam bandwidth when it is narrower than  $\delta v_\parallel \times \nu$ .

For the echo experiment the signal-to-noise ratio is optimized for an outgoing beam bandwidth equal or smaller than  $v_\parallel \times \nu$ . Using this critical value for the beam bandwidth, the echo power collected by the 21CMA detectors is

$$P_c = 6.7 \times 10^{-21} \text{ W} \left( \frac{g}{10^{-10} \text{ GeV}^{-1}} \right)^2 \times \left( \frac{100 \text{ MHz}}{\nu} \right) \left( \frac{P_0}{10 \text{ kW}} \right). \quad (6)$$

For such small values of the outgoing beam bandwidth, this power signal is concentrated in a frequency band identical to the one of the outgoing beam, but shifted by a value  $2v_\parallel \times \nu = 1.5 \times 10^{-3} \nu$ . The echo linewidth has a value  $\delta\nu_e = 26 \text{ kHz} \left( \frac{\nu}{50 \text{ MHz}} \right)$ , big enough to be resolved in the entire target frequency range.

We aim to cover the whole 21CMA frequency range, from 50 MHz to 200 MHz, in a time period of approximately two years. To do so, the number of outgoing beam shots that we need to send in one year is  $n = \nu/\delta\nu = 1923$ , each one with a duration of  $\tau = 1.64 \times 10^4$  s. To suppress the background, we would further employ an on-off technique, i.e., to switch on the beam for  $t_{\text{on}}$  and

<sup>2</sup> <http://21cma.bao.ac.cn>

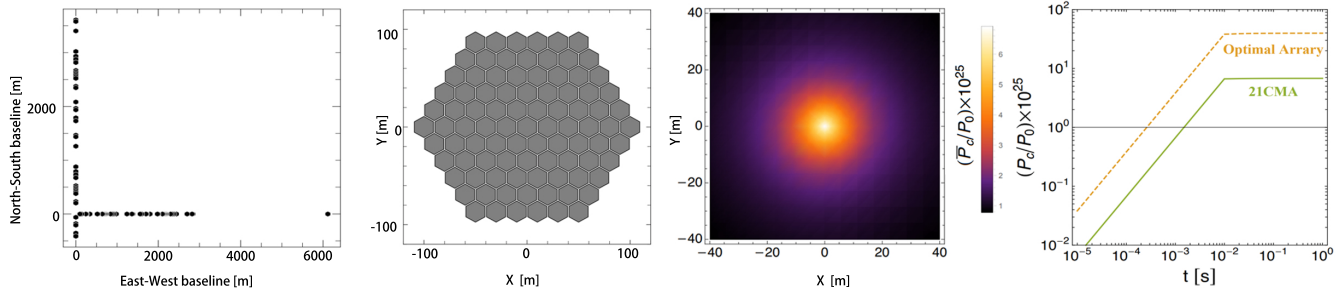


FIG. 2. (1) the current layout of the 21CMA array. (2) optimized layout (with additional 10 pods) for the axion echo experiment. (3) spatial distribution of the echo signal integrated over  $t_{\text{on}}$ . (4) axion echo time profiles for the current 21CMA layout (dashed) and the optimized layout (solid).

then switch off for another  $t_{\text{on}}$ . Thus the effective beam sending time for each shot is  $\tau_{\text{eff}} = 8205$  s.

We estimate the achievable sensitivity via a likelihood analysis by setting the outgoing beam to a periodic on-off mode. We generate simulation data based on the noise of the detector for the background-only hypothesis. The noise power of the detector array can be estimated as

$$P_{\text{noise}} = \frac{2k_B T_{\text{sys}} \delta\nu_e}{\sqrt{2\delta\nu_e \Delta t}}, \quad (7)$$

where  $T_{\text{sys}}$  is the system temperature,  $k_B$  is the Boltzmann constant, and  $\Delta t$  is the observing time. The  $\delta\nu_e$  factor appears in Eq. (7) because the echo bandwidth can be easily resolved by the detector. From now on we take it as  $\delta\nu_e = 5.2 \times 10^{-4} \nu$ . For the 21CMA,  $T_{\text{sys}}$  is approximately 300 K [63], which is the total noise temperature with contributions from the receiver, the antenna, the atmosphere, and the astrophysical background. Note that, using an on-off observation mode allows the quasi-constant part of the noise to be subtracted, leaving a fluctuation noise lower than  $T_{\text{sys}}$ , i.e., the thermal noise temperature of the 21CMA receiver which is about  $T_{\text{th}} = 50$  K [61, 62]. The resulting measurements are the power of the blank sky,  $P_i$ , with *rms* noise  $\sigma_i$ , where  $i$  denotes the time bin with width  $\Delta t_i$ . To calculate  $\sigma_i$ , we replace  $T_{\text{sys}}$  in Eq. (7) with  $T_{\text{th}} = 50$  K. We construct a  $\chi^2$  function as

$$\chi^2 = \sum_i \frac{[P_i - P_{\text{bkg},i} - \bar{P}_{\text{sig},i}(m_a, g)]^2}{\sigma_i^2}, \quad (8)$$

where  $P_{\text{bkg},i}$  is the background to be fitted in the analysis, and  $\bar{P}_{\text{sig},i}(m_a, g)$  is the average echo signal in the time bin  $\Delta t_i$

$$\bar{P}_{\text{sig},i}(m_a, g) = \frac{\int_{\Delta t_i} P(t) dt}{\Delta t_i}. \quad (9)$$

In the top panel of Fig. 3, we show the simulated data for the standard 21CMA layout and pure background hypothesis, compared with the echo signal from

an axion model with  $m_a = 0.83 \mu\text{eV}$  (corresponding to a frequency of axion induced electromagnetic wave of 100 MHz) and  $g = 3 \times 10^{-11} \text{ GeV}^{-1}$ . Here we assuming  $P_0 = 1 \text{ MW}$ ,  $t_{\text{on}} = 1 \text{ s}$  (to switch on the beam for  $t_{\text{on}}$  and then to switch off for another  $t_{\text{on}}$ ), with a time bin width of  $\Delta t_i = 0.02 \text{ s}$ . The integrated signal sending time is 8205 s, and the total experiment time is  $1.64 \times 10^4 \text{ s}$  for one frequency band with  $\delta\nu_c$  width. Varying the coupling constant  $g$ , we can get the  $\chi^2$  distribution as shown in the bottom panel of Fig. 3. Through setting the difference between  $\chi^2$  for any  $g$  and the minimum  $\chi_{\text{min}}^2$ ,  $\Delta\chi^2 = \chi^2 - \chi_{\text{min}}^2 = 2.71$ , we can get the 95% confidence level sensitivity on the axion-photon coupling for given mass  $m_a$ . For the above parameter setting, we get the 95% sensitivity on  $g$  to be  $9.5 \times 10^{-12} \text{ GeV}^{-1}$ . For the optimized layout as shown in Fig. 2, the signal will enhance by a factor of  $\sim 5.8$ , and hence the sensitivity on  $g$  will improve by a factor of  $\sqrt{5.8} = 2.4$ . We can further obtain the scaling relation between the sensitivity and the central frequency as  $g = 9.5 \times 10^{-12} (\nu/100 \text{ MHz})^{3/4} (P_0/\text{MW})^{-1/2} \text{ GeV}^{-1}$  for the standard 21CMA array, and  $g = 4.0 \times 10^{-12} (\nu/100 \text{ MHz})^{3/4} (P_0/\text{MW})^{-1/2} \text{ GeV}^{-1}$  for the optimized array.

#### IV. ENVIRONMENTAL AND BEAM CONTAMINATION

Electromagnetic waves suffer contamination from man-made radio frequency interference (RFI) and attenuation from the atmosphere and ionosphere. The long wavelength ( $< 1 \text{ GHz}$ ) signals are affected by interference from e.g., digital TV, FM, and communication signals of low-Earth-orbiting satellites [e.g. 66]. The site of 21CMA has a good radio environment, on the other hand, we take some strategies for RFI mitigation, which include: (1) placing electromagnetic shielding for each pod to minimize interference from neighbors and the ground; (2) skipping strong and steady RFI affecting channels; (3)

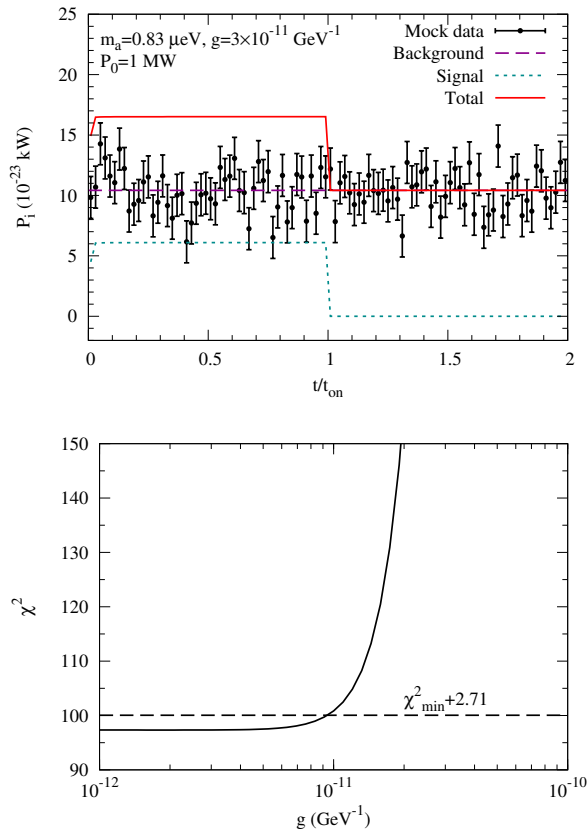


FIG. 3. Top: Simulated data for pure background hypothesis, folded for the whole  $1.64 \times 10^4$  s of operation. The current 21CMA layout is adopted. The horizontal dashed line is the average background, the blue dotted line corresponds to the echo signal for axions with  $m_a = 0.83 \mu\text{eV}$ ,  $g = 3 \times 10^{-11} \text{GeV}^{-1}$ , and an emitter power  $P_0 = 1 \text{MW}$ , and the red solid line is the sum of signal and background. Bottom:  $\chi^2$  versus axion-photon coupling  $g$ .

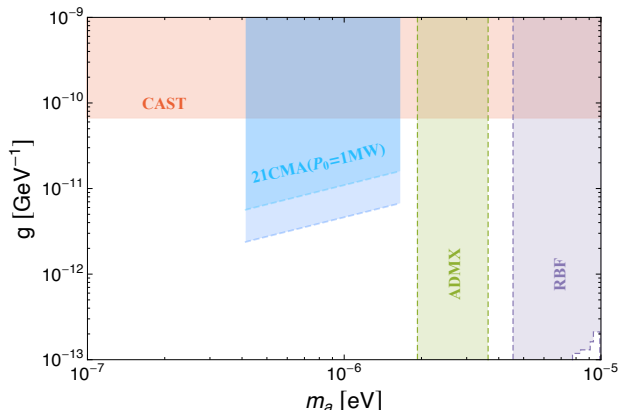


FIG. 4. Expected 90% C.L. sensitivity limits on the plane of the axion mass  $m_a$  and the axion-photon coupling  $g$ . We take the power of emitter  $P_0 = 1 \text{MW}$ . The bounds of CAST [64], ADMX [18], and RBF [65] are shown as well.

removing the instant RFI by using reference antennas; (4) flagging instant RFI in post-processing steps.

On the other hand, the ionosphere contributes the dominant contamination at the long wavelength ( $< 1 \text{GHz}$ ). The ionosphere is generally located from  $\sim 50$  to  $1000 \text{km}$  altitude over the Earth's surface, which causes both amplitude and phase errors via reflection and refraction, respectively. However, fortunately, ionospheric attenuation can be neglected by scheduling observations at night, which is primarily due to the absence of ionization from solar wind and radiation. The solar wind and radiation cause the ionosphere to become charged with electrons. At night, the recombination process in the ionosphere can suppress free electron contents down to 5% of its daily value [67]. Furthermore, there are already several methods to model and remove the influence from the ionosphere [see 68, and references therein].

It is also expected that the leakage of the emitter and the reflection of the beam in the ionosphere are strong sources of contamination. There are several possibilities to avoid this contamination. One way is to have a very narrow-band emitter (e.g., less than  $50 \text{kHz}$  for our benchmark case), the receive frequency will shift by about  $10^{-3}$  of the emitter central frequency. For instance, the echo frequency is shifted by about  $100 \text{kHz}$  with respect to a  $200 \text{MHz}$  emitter, meaning that, in frequency space, the signal is completely separated from the emitter and all contamination caused by itself. As a reference, the bandwidth coverage for the Sanya incoherent scatter radar site in Sanya, China, ranges from  $0.5 \text{kHz}$  to  $1 \text{MHz}$  [69]. The issue is that the scan efficiency is much lower than the wide-band emitter. The second way is to use on-off technique, i.e., to remove the data recorded during the emitting time. This way might be difficult since the echo signal comes dominantly from a distance of  $1e3$  times of the receiving array size ( $\sim 1000 \text{km}$  in our case), which has the order of magnitude of the height of the ionosphere. However, the ionosphere can also be avoided by pointing the beam in a different direction.

## V. CONCLUSIONS

The axion is a hypothetical elementary particle that could solve the long-standing strong CP problem in particle physics and the dark matter mystery in the cosmos. By sending radio waves to the space, the axion dark matter can be stimulated to generate a reflected signal and thus be detected by terrestrial telescopes. As a pathfinder, we study the expected sensitivity of searching for the axion dark matter between  $0.41$  and  $1.6 \mu\text{eV}$  with the 21 CentiMeter Array (21CMA). For a  $1 \text{MW}$  emitter covering the whole 21CMA frequency range in two years, we find that the resulting sensitivity on the axion-photon coupling surpasses helioscope bounds by about an order of magnitude.

## ACKNOWLEDGMENTS

A.A. thanks Nanjing Normal University for its hospitality while working on part of this paper. This work is supported by the National Natural Science Foundation

of China (12275134, 12147228, 12220101003, 12150010, 12103076, 12275232), the Project for Young Scientists in Basic Research of Chinese Academy of Sciences (No. YSBR-061) and the Ministry of Science and Technology of China (grant No. 2020SKA0110200).

- 
- [1] G. Bertone and D. Hooper, *Rev. Mod. Phys.* **90**, 045002 (2018), 1605.04909.
- [2] R. D. Peccei and H. R. Quinn, *Phys. Rev. Lett.* **38**, 1440 (1977).
- [3] J. E. Kim, *Phys. Rev. Lett.* **43**, 103 (1979).
- [4] M. A. Shifman, A. I. Vainshtein, and V. I. Zakharov, *Nucl. Phys. B* **166**, 493 (1980).
- [5] M. Dine, W. Fischler, and M. Srednicki, *Phys. Lett. B* **104**, 199 (1981).
- [6] A. R. Zhitnitsky, *Sov. J. Nucl. Phys.* **31**, 260 (1980).
- [7] P. Sikivie, *Lect. Notes Phys.* **741**, 19 (2008), astro-ph/0610440.
- [8] P. Svrcek and E. Witten, *JHEP* **06**, 051 (2006), hep-th/0605206.
- [9] A. Arvanitaki, S. Dimopoulos, S. Dubovsky, N. Kaloper, and J. March-Russell, *Phys. Rev. D* **81**, 123530 (2010), 0905.4720.
- [10] J. Preskill, M. B. Wise, and F. Wilczek, *Phys. Lett. B* **120**, 127 (1983).
- [11] L. Abbott and P. Sikivie, *Phys. Lett. B* **120**, 133 (1983).
- [12] M. Dine and W. Fischler, *Phys. Lett. B* **120**, 137 (1983).
- [13] D. J. E. Marsh, *Phys. Rept.* **643**, 1 (2016), 1510.07633.
- [14] A. D. Linde and D. H. Lyth, *Phys. Lett. B* **246**, 353 (1990).
- [15] D. H. Lyth, *Phys. Rev. D* **45**, 3394 (1992).
- [16] P. Arias, D. Cadamuro, M. Goodsell, J. Jaeckel, J. Redondo, and A. Ringwald, *JCAP* **06**, 013 (2012), 1201.5902.
- [17] R. Khatiwada et al. (ADMX), *Rev. Sci. Instrum.* **92**, 124502 (2021), 2010.00169.
- [18] C. Bartram et al. (ADMX), *Phys. Rev. Lett.* **127**, 261803 (2021), 2110.06096.
- [19] T. Braine et al. (ADMX), *Phys. Rev. Lett.* **124**, 101303 (2020), 1910.08638.
- [20] N. Du et al. (ADMX), *Phys. Rev. Lett.* **120**, 151301 (2018), 1804.05750.
- [21] M. J. Jewell et al. (HAYSTAC), *Phys. Rev. D* **107**, 072007 (2023), 2301.09721.
- [22] A. K. Yi et al., *Phys. Rev. Lett.* **130**, 071002 (2023), 2210.10961.
- [23] C. M. Adair et al., *Nature Commun.* **13**, 6180 (2022), 2211.02902.
- [24] D. Alesini et al., *Phys. Rev. D* **106**, 052007 (2022), 2208.12670.
- [25] C. P. Salemi et al., *Phys. Rev. Lett.* **127**, 081801 (2021), 2102.06722.
- [26] A. V. Gramolin, D. Aybas, D. Johnson, J. Adam, and A. O. Sushkov, *Nature Phys.* **17**, 79 (2021), 2003.03348.
- [27] J. A. Devlin et al., *Phys. Rev. Lett.* **126**, 041301 (2021), 2101.11290.
- [28] Y. Oshima, H. Fujimoto, J. Kume, S. Morisaki, K. Nagano, T. Fujita, I. Obata, A. Nishizawa, Y. Michimura, and M. Ando (2023), 2303.03594.
- [29] A. Arza, M. A. Fedderke, P. W. Graham, D. F. J. Kimball, and S. Kalia, *Phys. Rev. D* **105**, 095007 (2022), 2112.09620.
- [30] I. A. Sulai et al. (2023), 2306.11575.
- [31] I. M. Bloch and S. Kalia (2023), 2308.10931.
- [32] P. Brun et al. (MADMAX), *Eur. Phys. J. C* **79**, 186 (2019), 1901.07401.
- [33] L. Brouwer et al. (DMRadio), *Phys. Rev. D* **106**, 103008 (2022), 2204.13781.
- [34] T. Grenet, R. Ballou, Q. Basto, K. Martineau, P. Perrier, P. Pugnât, J. Quevillon, N. Roch, and C. Smith (2021), 2110.14406.
- [35] M. Lawson, A. J. Millar, M. Pancaldi, E. Vitagliano, and F. Wilczek, *Phys. Rev. Lett.* **123**, 141802 (2019), 1904.11872.
- [36] J. Liu et al. (BREAD), *Phys. Rev. Lett.* **128**, 131801 (2022), 2111.12103.
- [37] M. Baryakhtar, J. Huang, and R. Lasenby, *Phys. Rev. D* **98**, 035006 (2018), 1803.11455.
- [38] A. Berlin, R. T. D’Agnolo, S. A. R. Ellis, and K. Zhou, *Phys. Rev. D* **104**, L111701 (2021), 2007.15656.
- [39] B. Giaccone et al. (2022), 2207.11346.
- [40] D. J. E. Marsh, K.-C. Fong, E. W. Lentz, L. Smejkal, and M. N. Ali, *Phys. Rev. Lett.* **123**, 121601 (2019), 1807.08810.
- [41] J. Schütte-Engel, D. J. E. Marsh, A. J. Millar, A. Sekine, F. Chadha-Day, S. Hoof, M. N. Ali, K.-C. Fong, E. Hardy, and L. Šmejkal, *JCAP* **08**, 066 (2021), 2102.05366.
- [42] Z. Zhang, D. Horns, and O. Ghosh, *Phys. Rev. D* **106**, 023003 (2022), 2111.04541.
- [43] P. Sikivie, *Rev. Mod. Phys.* **93**, 015004 (2021), 2003.02206.
- [44] I. G. Irastorza and J. Redondo, *Prog. Part. Nucl. Phys.* **102**, 89 (2018), 1801.08127.
- [45] A. Caputo, M. Regis, M. Taoso, and S. J. Witte, *JCAP* **03**, 027 (2019), 1811.08436.
- [46] A. Arza, T. Schwetz, and E. Todarello, *JCAP* **10**, 013 (2020), 2004.01669.
- [47] A. Arza, *Eur. Phys. J. C* **79**, 250 (2019), 1810.03722.
- [48] G. Alonso-Álvarez, R. S. Gupta, J. Jaeckel, and M. Spannowsky, *JCAP* **03**, 052 (2020), 1911.07885.
- [49] P. Arias, A. Arza, J. Jaeckel, and D. Vargas-Arancibia, *JCAP* **05**, 070 (2021), 2007.12585.
- [50] A. Arza and P. Sikivie, *Phys. Rev. Lett.* **123**, 131804 (2019), 1902.00114.
- [51] A. Arza and E. Todarello, *Phys. Rev. D* **105**, 023023 (2022), 2108.00195.
- [52] M. A. Buen-Abad, J. Fan, and C. Sun, *Phys. Rev. D* **105**, 075006 (2022), 2110.13916.
- [53] Y. Sun, K. Schutz, A. Nambrath, C. Leung, and K. Masui, *Phys. Rev. D* **105**, 063007 (2022), 2110.13920.
- [54] O. Ghosh, J. Salvado, and J. Miralda-Escudé (2020), 2008.02729.

- [55] K. A. Beyer, G. Marocco, R. Bingham, and G. Gregori, *Phys. Rev. D* **105**, 035031 (2022), 2109.14663.
- [56] L. D. Duffy and P. Sikivie, *Phys. Rev. D* **78**, 063508 (2008), 0805.4556.
- [57] S. S. Chakrabarty, Y. Han, A. H. Gonzalez, and P. Sikivie, *Phys. Dark Univ.* **33**, 100838 (2021), 2007.10509.
- [58] Y. Gong, X. Liu, L. Wu, Q. Yang, and B. Zhu (2023), 2308.08477.
- [59] A. Arza, A. Kryemadhi, and K. Zioutas (2022), 2212.10905.
- [60] M. Vogelsberger and S. D. M. White, *Mon. Not. Roy. Astron. Soc.* **413**, 1419 (2011), 1002.3162.
- [61] Y. Huang, X.-P. Wu, Q. Zheng, J.-H. Gu, and H. Xu, *Research in Astronomy and Astrophysics* **16**, 36 (2016), 1602.06623.
- [62] Q. Zheng, X.-P. Wu, M. Johnston-Hollitt, J.-h. Gu, and H. Xu, *Astrophys. J.* **832**, 190 (2016), 1602.06624.
- [63] J. Wang, H. Xu, T. An, J. Gu, X. Guo, W. Li, Y. Wang, C. Liu, O. Martineau-Huynh, and X.-P. Wu, *Astrophys. J.* **763**, 90 (2013), 1211.6450.
- [64] V. Anastassopoulos et al. (CAST), *Nature Phys.* **13**, 584 (2017), 1705.02290.
- [65] S. DePanfilis, A. C. Melissinos, B. E. Moskowitz, J. T. Rogers, Y. K. Semertzidis, W. U. Wuensch, H. J. Hallama, A. G. Prodel, W. B. Fowler, and F. A. Nezrick, *Phys. Rev. Lett.* **59**, 839 (1987), URL <https://link.aps.org/doi/10.1103/PhysRevLett.59.839>.
- [66] A. R. Offringa, R. B. Wayth, N. Hurley-Walker, D. L. Kaplan, N. Barry, A. P. Beardsley, M. E. Bell, G. Bernardi, J. D. Bowman, F. Briggs, et al., *Publ. Astron. Soc. Aust.* **32**, e008 (2015), 1501.03946.
- [67] F. de Gasperin, M. Mevius, D. A. Rafferty, H. T. Intema, and R. A. Fallows, *Astron. Astrophys.* **615**, A179 (2018), 1804.07947.
- [68] H. T. Intema, S. van der Tol, W. D. Cotton, A. S. Cohen, I. M. van Bemmelen, and H. J. A. Röttgering, *Astron. Astrophys.* **501**, 1185 (2009), 0904.3975.
- [69] X. Yue, W. Wan, B. Ning, L. Jin, F. Ding, B. Zhao, L. Zeng, C. Ke, X. Deng, J. Wang, et al., *Journal of Geophysical Research (Space Physics)* **127**, e30451 (2022).